

PAPER • OPEN ACCESS

Inclusions of a two dimensional fluid with competing interactions in a disordered, porous matrix

To cite this article: Cecilia Bores *et al* 2015 *J. Phys.: Condens. Matter* **27** 194127

View the [article online](#) for updates and enhancements.

Related content

- [Phase separation in confined systems](#)
Lev D Gelb, K E Gubbins, R Radhakrishnan *et al.*
- [Static structure of active Brownian hard disks](#)
N de Macedo Binossek, H Löwen, Th Voigtmann *et al.*
- [Vapour-liquid phase diagram for an ionic fluid in a random porous medium](#)
M F Holovko, O Patsahan and T Patsahan

Recent citations

- [Scaled particle theory for bulk and confined fluids: A review](#)
Wei Dong and XiaoSong Chen
- [Fluids in porous media. IV. Quench effect on chemical potential](#)
C. Z. Qiao *et al*

Inclusions of a two dimensional fluid with competing interactions in a disordered, porous matrix

Cecilia Bores¹, Noé G Almarza¹, Enrique Lomba¹ and Gerhard Kahl²

¹ Instituto de Química Física Rocasolano, CSIC, Calle Serrano 119, E-28026 Madrid, Spain

² Institut für Theoretische Physik and Center for Computational Materials Science (CMS), Technische Universität Wien, Wiedner Hauptstraße 8-10, A-1040 Wien, Austria

E-mail: cbores@iqfr.csic.es

Received 2 October 2014, revised 18 November 2014

Accepted for publication 2 December 2014

Published 29 April 2015



CrossMark

Abstract

The behavior of a fluid with competing interaction ranges adsorbed in a controlled pore size disordered matrix is studied by means of grand canonical Monte Carlo simulations in order to analyze the effects of confinement. The disordered matrix model is constructed from a two-dimensional non-additive hard-sphere fluid (which shows close to its demixing critical point large fluctuations in the concentration), after a subsequent quenching of the particle positions and removal of one of the components. The topology of the porous network is analyzed by means of a Delaunay tessellation procedure. The porous cavities are large enough to allow for cluster formation, which is however somewhat hindered as a result of the confinement, as seen from the comparison of cluster size distributions calculated for the fluid under confinement and in the bulk. The occurrence of lamellar phases is impeded by the disordered nature of the porous network. Analysis of two-dimensional density maps of the adsorbed fluid for given matrix configurations shows that clusters tend to build up in specific locations of the porous matrix, so as to minimize inter-cluster repulsion.

Keywords: fluids with competing interactions, disordered, porous matrix, adsorption

(Some figures may appear in colour only in the online journal)

1. Introduction

The description of adsorption processes of complex fluids on disordered, porous matrices using theoretical concepts and/or computer simulations is of paramount importance in many fields of technological relevance, such as heterogeneous catalysis, gas storage, molecular sieving, or gas chromatography, to name a few [1, 2]. If one aims at a *quantitative* prediction of such processes, it is indispensable to mimic in the underlying theoretical models the features both of the matrix as well as of the adsorbed fluid as faithfully as possible.

As a typical, widespread material of such a matrix we consider a controlled pore size glass, e.g. a borosilicate glass whose precursor is typically a mixture of $\text{Na}_2\text{O}-\text{B}_2\text{O}_3-\text{SiO}_2$, which shows a characteristic miscibility gap for certain compositions [3]: in this material the typical pore size ranges between 1 nm and 1 μm , the glass shows as a consequence of the rigid silica network a high degree of chemical, thermal and mechanical stability and the inner surface of the material can easily be functionalized. The production of such a porous glass is realized in what is known as the VYCOR process [3, 4]: after thermal treatment a glass is formed via spinodal decomposition into a sodium-rich borate phase and a silica phase; removing in a subsequent step the former one, leaving a highly porous, disordered matrix with the above-mentioned properties. Characteristic features of the emerging glass (such as porosity, pore size, etc) can be influenced by



Content from this work may be used under the terms of the [Creative Commons Attribution 3.0 licence](https://creativecommons.org/licenses/by/3.0/). Any further distribution of this work must maintain attribution to the author(s) and the title of the work, journal citation and DOI.

the thermal treatment and/or the original composition of the material.

In an effort to capture the main features of this process in an *in silico* preparation of the matrix, we use in our investigations the simplest possible system that shows spinodal decomposition, namely a binary mixture of (positively) non-additive hard spheres. In order to enhance the visibility of our results we restrict ourselves to a two-dimensional system. Using semi-grand canonical Monte Carlo simulations we generate particle configurations of our mixture close to the critical density where concentration fluctuations are pronounced. Selecting suitable configurations and removing one particle species we mimic the essential features of the above outlined VYCOR process, leading finally to our matrix configurations. A subsequent analysis of those areas that are accessible to an added fluid in terms of a Delaunay triangulation [5–8] provides quantitative information about the characteristic features of the matrix, such as the porosity and the pore size distribution.

We then bring a specific fluid into contact with the matrix and study its adsorption behavior. Despite the simplicity of the model fluid, it is able to show a rather complex phase behavior in terms of mesophase formation. Originally introduced by Sear and co-workers [9] to model the interaction of nanoparticles at the air-water interface, the potential action between the particles of the system is characterized by a strongly repulsive region plus an adjacent tail that is attractive at short distances and repulsive at intermediate and long distances (SALR). As a consequence of the intricate interplay of the attractive and the repulsive components of the interaction, the system is able to form mesophases below a certain temperature: with increasing density clusters, stripes and inverse clusters (i.e. bubbles) emerge [10–12]. Thus, this simple model is able to mimic characteristic self-assembly features of realistic systems, such as food, pharmaceuticals, vegetation patterns, etc [13–18].

Using grand canonical Monte Carlo (GCMC) simulations we study the behavior of the SALR fluid inclusions in the disordered matrix for various chemical potentials (i.e. fluid densities) and temperatures. We investigate the effects of disorder and simple geometric confinement, since the matrix-fluid interactions are modeled by plain hard-core repulsions. Particle aggregation is characterized by means of a cluster analysis of the fluid configurations and the presence of a pre-peak in the fluid structure factor which grows as temperature is lowered. The temperature-density region where clustering is dominant under confinement is compared with that of the corresponding bulk system. No evidence of the presence of fluid lamellar phases is found, in contrast to the behavior previously described for this SALR fluid in bulk [11] and in particular under slit pore confinement [12]. With the aid of two-dimensional density maps, one can see that clustering builds up at specific locations in the pore topology in an effort to minimize inter-cluster repulsion.

The manuscript is organized as follows: in the subsequent section we present our model, putting particular emphasis on the *in silico* production process of our matrix that mimics features of the VYCOR process; furthermore, we introduce

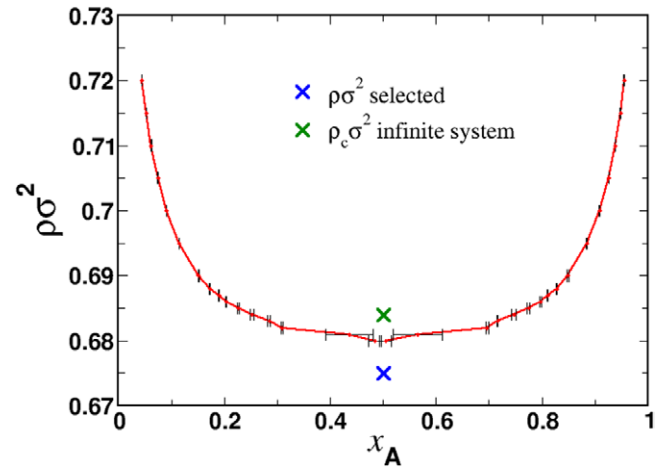


Figure 1. Phase diagram of a two-dimensional, binary mixture of non-additive hard spheres in the (ρ, x_A) -plane as obtained from semi-grand canonical MC simulations, applying histogram reweighting techniques (see text). An estimate for the critical density, ρ_c (see text), is indicated by the green cross. The blue cross specifies the ρ -value that has been considered in subsequent investigations for possible matrix configurations. Error bars provide evidence of the accuracy of the data along the coexistence curve.

our model for the complex fluid. In section 3 we present and discuss our results and close the manuscript in section 4 with a summary and an outlook to future work.

2. Model and methods

2.1. The matrix

For our theoretical investigations we want to create a matrix that mimics the experimental preparation process of a realistic controlled pore glass as faithfully as possible [19]. Since spinodal decomposition [20] (and subsequent removal of one of the components) is a standard process in experimental matrix synthesis processes, we proceed in our theoretical approach along similar lines. To this end we consider a two-dimensional, binary mixture of non-additive hard spheres: such a system is easily accessible from the computational point of view and is able to show for certain system parameter combinations spinodal decomposition. Thus, we expect that our *in silico* matrix will capture the most relevant features of a realistic matrix.

In our binary mixture of non-additive hard spheres the diameters of both species (labeled ‘A’ and ‘B’) are assumed to be equal ($\sigma_{AA} = \sigma_{BB} = \sigma$), while we set cross-interaction diameter, σ_{AB} , to

$$\sigma_{AB} = \frac{1}{2}(1 + \Delta)(\sigma_{AA} + \sigma_{BB}).$$

σ is used henceforward as the unit length. Setting $\Delta = 0.2$, the system undergoes above a certain critical density, ρ_c , a demixing transition [21]. Later on, one of the two particle species will play the role of matrix particles (in our case it will be species A) while the other species acts as a template and is to be removed creating thereby the pores of our matrix.

For this binary mixture we have performed semi-grand canonical Monte Carlo (MC) simulations [22, 23], imposing the difference in chemical potential $\Delta\mu = \mu_A - \mu_B$ between

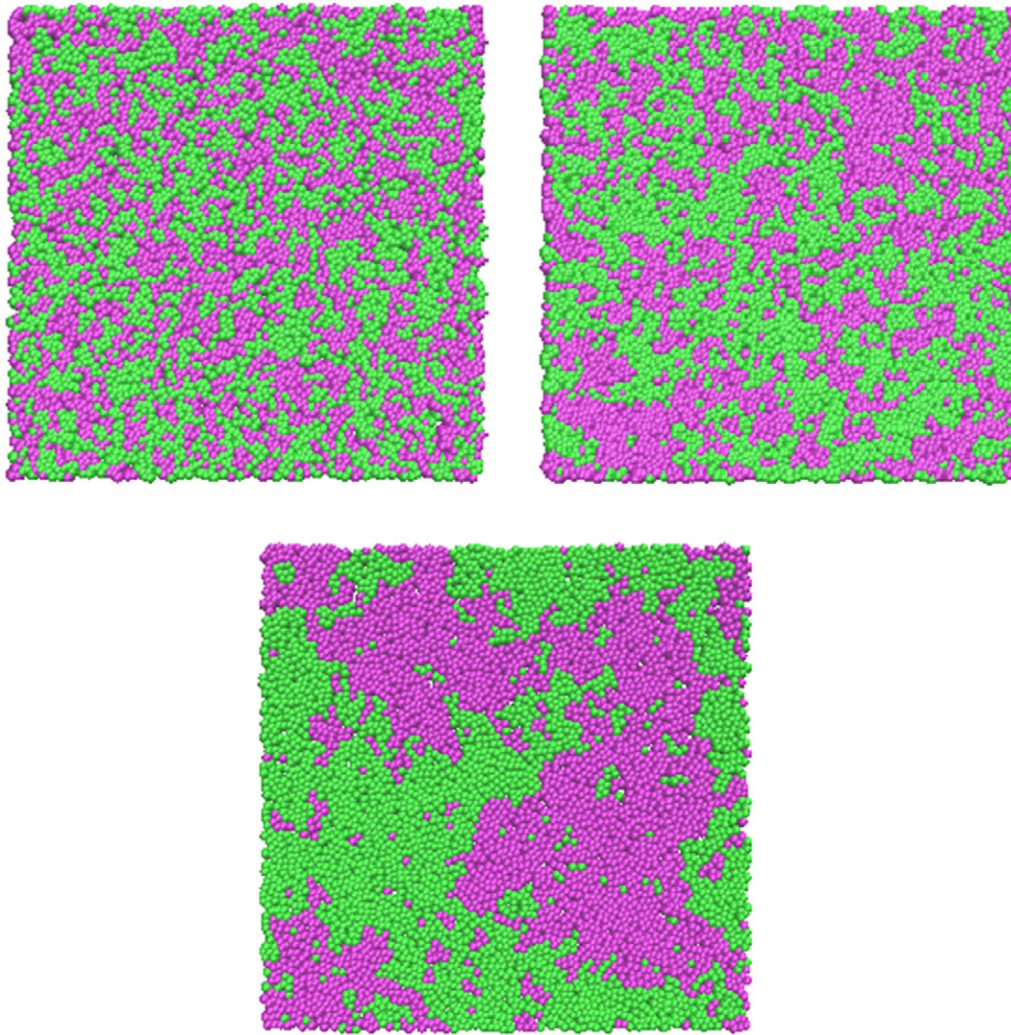


Figure 2. Typical snapshots of our two-dimensional binary mixture of non-additive hard spheres as obtained in MC simulations (see text). Particles of the two species are depicted in different colors. The respective values for the overall number density, ρ , are $\rho\sigma^2 = 0.5, 0.6$ and 0.675 (from left to right and from top to bottom).

species A and B, the area $A(= L^2)$ with L being the edge length of the quadratic simulation box, the temperature T and keeping the total number of particles, $N(= N_A + N_B)$ fixed; $x_A = N_A/N$ is the concentration of particles of species A. The total number density $\rho = N/A$ is thus fixed. In addition to the conventional MC moves, particles can also exchange their identity in suitable MC moves [24]. After 5×10^5 MC sweeps for equilibration, our simulations were typically extended over 10^6 MC sweeps.

Analyzing the molar fraction histograms for the binary mixture for different densities and system sizes, the concentrations at coexistence, $x_A(\rho)$ and thus the phase diagram of the system could be evaluated; it is depicted in the (ρ, x_A) -plane in figure 1. In an effort to locate the critical density ρ_c of the demixing transition as accurately as possible we have considered different ensemble sizes with N varying between 5000 and 20000 particles. Using the scaling laws given in [25], the value of the critical density for an *infinite* system size is estimated to be $\rho_c = 0.684$. For density-values close to the critical density the system exhibits strong fluctuations in x_A (and thus in N_A), a fact that will be of

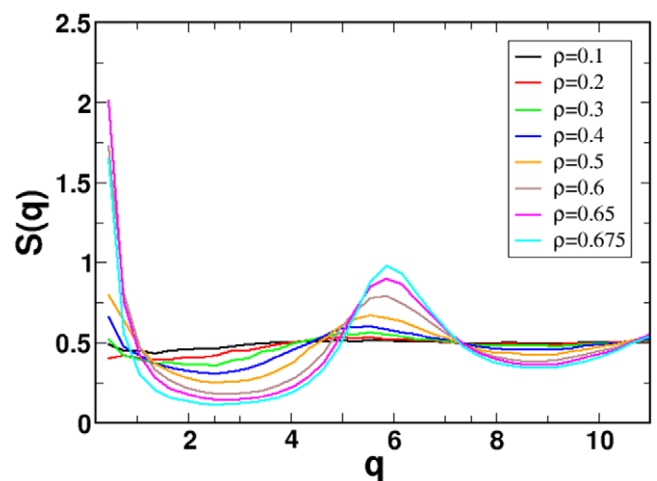


Figure 3. (Partial) structure factor of particle species A, $S(q)$, as a function of q of our two-dimensional, binary mixture of non-additive hard spheres as obtained in MC simulations (see text), evaluated for different values of the overall number density, $\rho\sigma^2$ (as labeled).

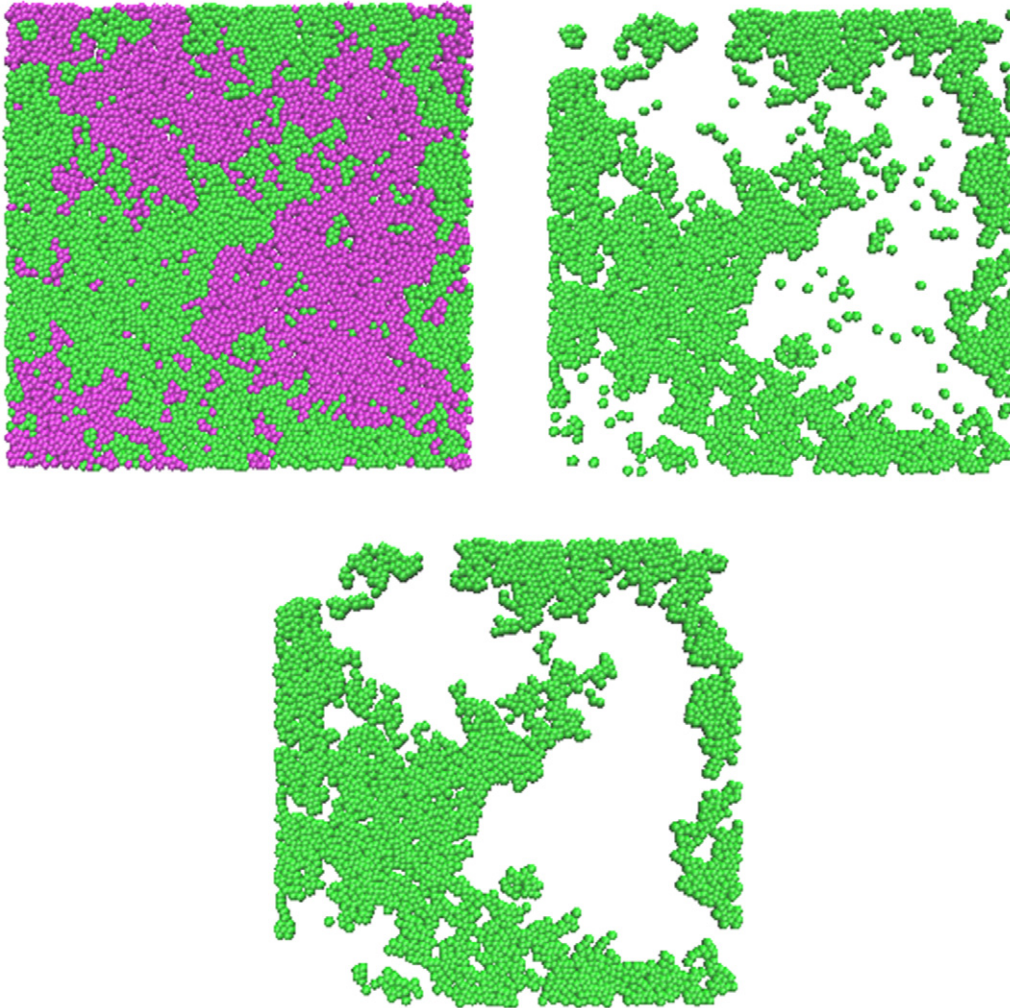


Figure 4. Visualization of the creation process of a matrix configuration. Top-left panel: typical snapshot of our two-dimensional, binary mixture of non-additive hard spheres close to spinodal decomposition conditions; particles of the two species are depicted in different colors (species A—light; species B—dark). Top-right panel: particles of species B have been removed. Bottom panel: particles of species A that are located in isolated parts within areas predominantly populated by particles of species B are removed, leaving the remaining particle species A as the desired matrix configuration.

relevance when creating a matrix of desired density, ρ_m and porosity (see below). Thus, it is appropriate to retain at this point candidate matrix configurations with a number of matrix particles that roughly corresponds to the desired target value of the matrix density.

In figure 2 we show typical snapshots of particle configurations as obtained in our simulations of the binary mixture for selected ρ -values. The corresponding (partial) structure factor $S(q)$ for the A-particles is depicted in figure 3; these functions show—upon approaching the critical density—the expected onset of a divergence at small q -values, a feature characteristic for a system close to spinodal decomposition. Alternatively, thinking in terms of the final matrix-scattering factor, the low- q divergence in the structure factor is a direct result of the presence of pores with length scales comparable to the simulation box size. The low- q behavior can be related to the surface of the pore network and its structure, a much used approach in the analysis of small angle diffraction data in porous materials [26].

From these particle configurations we can now construct our matrix via a process that is schematically depicted in the

panels of figure 4 and that will be outlined in the following. Let us assume that our simulation-generated configuration contains a suitable number of A-particles; a representative particle arrangement is shown in the top-left panel of figure 4. We now remove all particles of species B, a procedure that corresponds to etching out a particular component in the experimental matrix synthesis process (see top-right panel of figure 4). Finally, we have to remove all those isolated A-particles, that are separated from regions covered by a network of A-particles by a distance larger than some cut-off value; for our purposes this cut-off distance was assumed to be 2σ . Thus, we end up with a compact matrix formed by A-particles (see bottom panel of figure 4). We note that a similar procedure has been used to create the matrix in a related problem [27].

With such a matrix configuration at hand we can now proceed to the characterization and to the analysis of the porous structure on a quantitative level, based on a Delaunay decomposition of the simulation cell [6]. Starting from the positions of the matrix particles (top-left panel of figure 5), Delaunay triangles are constructed (top-right panel of figure 5)

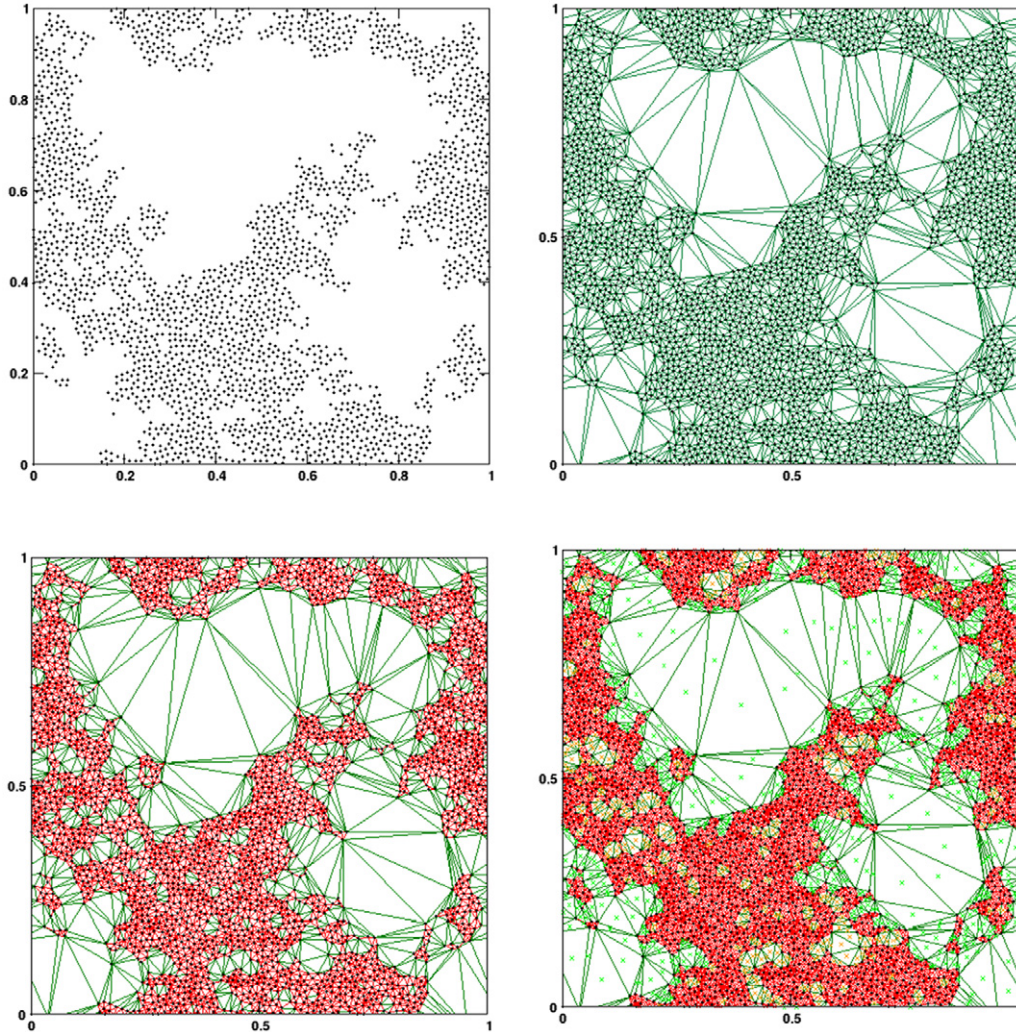


Figure 5. Quantitative analysis of a representative matrix configuration (depicted in figure 4) based on a Delaunay decomposition. Top-left panel: points represent positions of the matrix particles; top-right panel: Delaunay decomposition based on these positions; bottom-left panel: crossable (green) and non-crossable (red) edges of the Delaunay triangles (see text); bottom-right panel: accessible and non-accessible Delaunay triangles are marked by a green and a red point in their center, respectively.

via a well-defined process [7, 8, 28]. The edges of these triangles are now classified either as ‘crossable’ faces (i.e. they are sufficiently long to let particles of diameter σ pass) or as ‘non-crossable’ faces (i.e. they are shorter than σ); the respective faces are colored in the bottom-left panel of figure 5 in green or red, respectively. Delaunay triangles that have only non-crossable faces have to be discarded for obvious reasons and we are finally left with Delaunay triangles with crossable faces only *and* that can be reached by the fluid particles by diffusion and inclusion (bottom-right panel of figure 5). The total area covered by accessible Delaunay triangles in relation to the total surface of the simulation cell yields the porosity parameter p , with $0 \leq p \leq 1$. Repeating the creation process of the matrix and its analysis in terms of a Delaunay decomposition several hundred times, we obtain a narrow probability distribution of the porosity parameter p of all the created matrices centered around a porosity value of $p \simeq 47\%$. We note in passing that the composition of the original sample prior to quenching and removal of B particles is far from being equimolar (which explains why the portion of solid material

in the matrix is above 50%). This is simply due to the fact that during the semi-grand ensemble simulation the composition necessarily fluctuates.

2.2. The fluid

In the following, we immerse a fluid of a desired density, ρ_f , at a target temperature T into this matrix. The fluid particles interact via a potential $\Phi(r)$; this interaction consists of a repulsive region (with a spatial extent σ) and is characterized beyond this region by a tail that is attractive at short distances and repulsive at larger particle separations. In this contribution we have chosen a slightly modified version of the standard parameterization for this type of interaction, introduced previously by Sear *et al* [9] and analyzed in detail by Imperio and Reatto [10–12], with the following functional form:

$$\Phi(r) = -\epsilon_a \frac{\sigma^2}{R_a^2} \exp\left(-\frac{r}{R_a}\right) + \epsilon_r \frac{\sigma^2}{R_r^2} \exp\left(-\frac{r}{R_r}\right) + u_{sr}(r) \quad (1)$$

ϵ_a (ϵ_r) and R_a (R_r) represent the strength and the range of the attractive (repulsive) contribution to the potential tail in $\Phi(r)$, respectively. The short range repulsive part of $\Phi(r)$ is given by

$$u_{sr}(r) = \left(\frac{\sigma + \delta}{r} \right)^n \quad (2)$$

with $n = 20$ and $\delta = -0.01\sigma$. This soft-core repulsion replaces the hard-core term used in [10–12] in order to ease forthcoming studies on dynamic properties by means of molecular dynamics simulations. For computational convenience all interactions are cut and shifted at $R_c = 10\sigma$.

In our case we have chosen the following potential parameters: $R_a = \sigma$, $R_r = 2\sigma$ and $\epsilon = \epsilon_a = \epsilon_r$. Our decision to use these particular values for the potential parameters is based on the fact that they have been used in previous studies of SALR fluids [10–12, 29, 30]. The cutoff radius is chosen large enough to preserve the clustering behavior. Increasing this cutoff would only imply somewhat larger inter-cluster separations, since the cutoff is located in the repulsive tail of interaction.

Furthermore, we introduce the dimensionless temperature, $T^* = k_B T / \epsilon$, k_B being the Boltzmann constant. The potential $\Phi(r)$ is depicted for this particular choice of parameters in figure 6.

Depending on the density and the temperature this system is able to show a rich phase behavior, which is characterized below a certain temperature by the formation of three archetypes of mesophases: clusters (at low densities), stripes (at intermediate densities) and bubbles (i.e. inverse clusters at high densities). Typical snapshots for the equilibrated (i.e. unconfined) system as obtained in computer simulations are shown in figure 7 together with structural information in the form of pair distribution functions $g(r)$ and static structure factors $S(q)$. The phase behavior of this system has been studied quite extensively during recent years [10–12, 29–32].

3. Results

The aim of this paper is to study the influence of confinement realized via a disordered, porous matrix on the properties of a fluid with competing interactions: among others we will address the question of how the characteristic pattern formations of these particles will be affected by the confinement.

Using GCMC simulations (i.e. in an μAT -ensemble) we have studied the structural and thermodynamic properties of both the bulk and the confined SALR fluid. Simulations have been realized in a square simulation box of area $A = L^2$ using periodic boundary conditions. In the case of the bulk fluid we have used $L = 64\sigma$ and $L = 86\sigma$ for the confined system. When comparing values of the densities of the bulk and of the confined fluid (ρ_f), in the latter case we refer to the *effective* density of the adsorbed fluid, evaluated as the number of fluid particles per area of the accessible matrix sample. Densities reported correspond to averages along the simulation runs and have standard deviations that vary typically in the range of 1–3%.

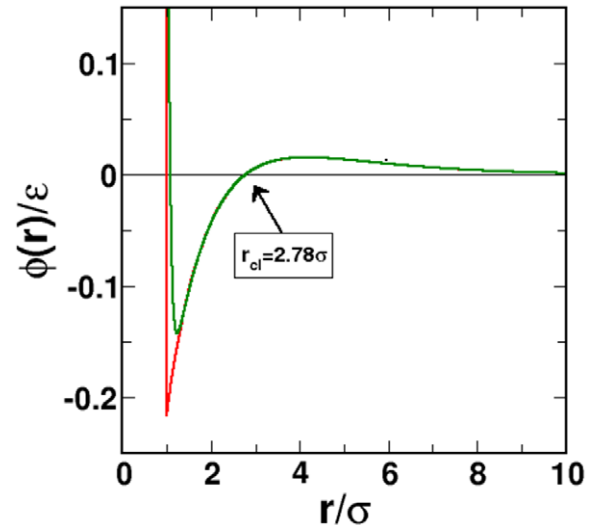


Figure 6. Interaction potential $\Phi(r)$ as a function of the distance r . The red line shows the original SALR potential as used in [10, 11] with the parameters specified in the text; the green line denotes the softened version of the SALR potential used in this contribution and as specified in equations (1) and (2). The distance r_{cl} highlighted in the figure corresponds to $\Phi(r_{cl}) = 0$ and defines our reference distance to consider two particles linked in a cluster.

Since matrix-fluid interactions are plain hard-core repulsions, we can anticipate that any deviations in the behavior of the confined fluid with respect to the properties of the bulk fluid will originate from the effects of randomness and the topology of the confining matrix.

3.1. Thermodynamic properties

In figure 8 we show the adsorption isotherms (i.e. the chemical potential $\mu/k_B T$) and the potential energy E versus the fluid density ρ_f for several temperatures ranging from $T^* = 0.09$ to $T^* = 0.33$, corresponding to state points where cluster formation is observed. Results for the bulk and for the confined fluid (at a matrix density $\rho_m \sigma^2 = 0.324$) are shown and compared in figure 8. We observe that the chemical potential attains lower values for the same density when the fluid is confined. This effect is likely the result of the presence of long range repulsions between fluid particles, whose net impact is diminished by the presence of matrix particles. Effects of clustering are visible in the energy at low temperature: the energy curves exhibit a minimum and then bend upwards as the density is increased ($\rho_f \sigma^2 \gtrsim 0.15$ in the bulk and $\rho_f \sigma^2 \gtrsim 0.23$ under confinement) due to the effect of increasingly dominant inter-cluster repulsions. The presence of the matrix shifts the effect of long-ranged interparticle repulsion to a higher fluid density value and the potential energy remains negative over all the density range considered. These features are most likely due to the effect of the spatial separation forced upon the fluid particles as a consequence of the presence of matrix. One might expect on this basis that the cluster phase will be stable even up to higher densities in the confined system. This will become evident in the next subsection when plotting the structural phase diagram.

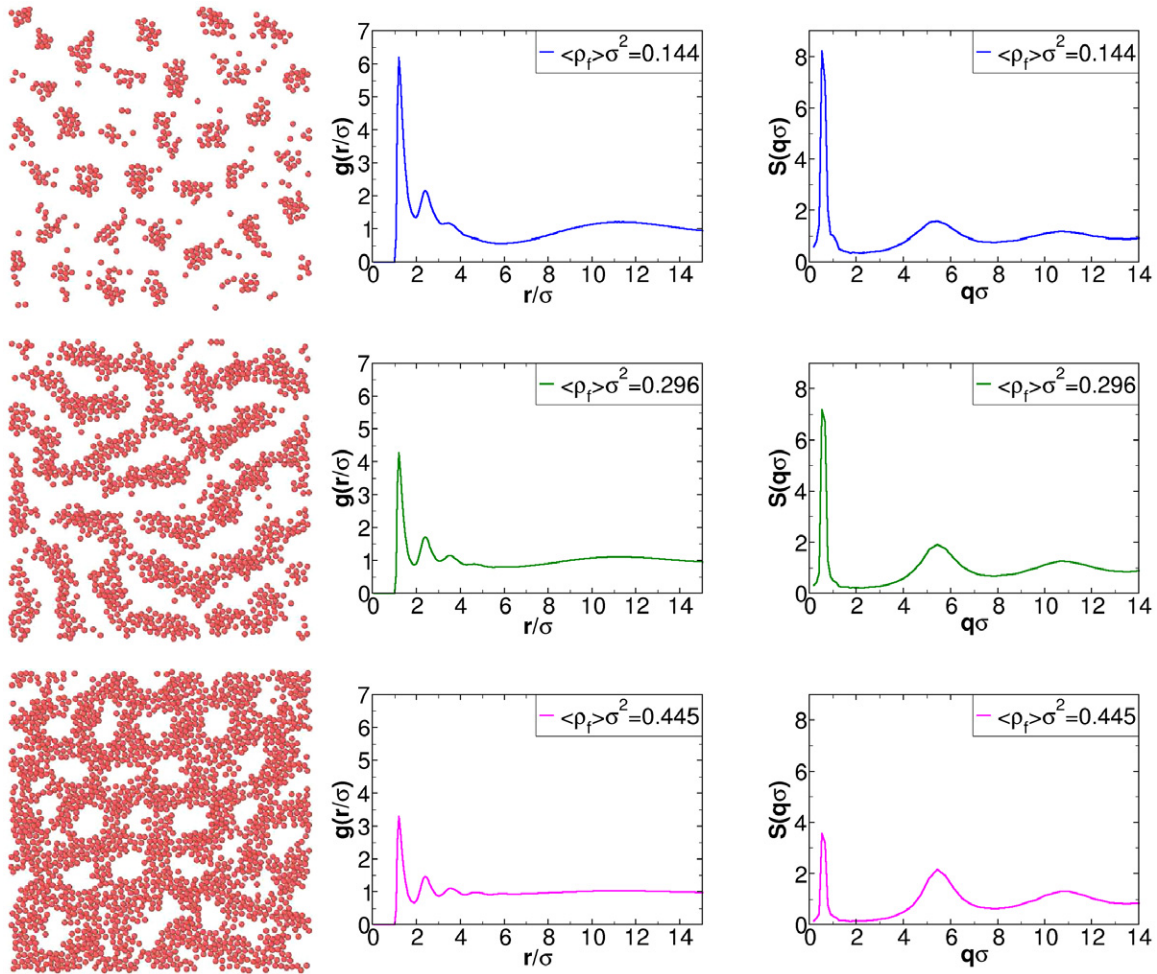


Figure 7. Left panels: typical snapshots of a two-dimensional system where the particles interact via a potential given in equations (1) and (2) using parameters specified in the text; results were obtained in GCMC simulations. The temperature was set to $T^* = 0.09$; snapshots were taken at different densities (from top to bottom $\langle \rho_f \rangle \sigma^2 = 0.144$, $\langle \rho_f \rangle \sigma^2 = 0.2955$ and $\langle \rho_f \rangle \sigma^2 = 0.4454$). Central panels: corresponding pair distribution functions $g(r)$ as functions of r . Right panels: static structure factors $S(q)$ as functions of q .

3.2. Structural properties

We have studied the characteristic mesophases that occur in the SALR fluid in bulk (namely droplets, stripes and bubbles [10, 11]) and have investigated to what extent they appear in the confined geometry. First, we have performed a qualitative, visual inspection of the typical snapshots, followed by a more quantitative analysis in terms of pair distribution functions, $g(r)$ and structure factors, $S(q)$. These results are collected in figure 7 for the bulk fluid and in figure 9 for the confined fluid.

We start our discussion with the bulk case: in the left column of figure 7 one can see in representative snapshots of the system taken at a sufficiently low temperature ($T^* = 0.09$) that particles self-assemble into the characteristic mesophases and for appropriate fluid densities: $\langle \rho_f \rangle \sigma^2 = 0.14401$ (droplets), $\langle \rho_f \rangle \sigma^2 = 0.29551$ (stripes) and $\langle \rho_f \rangle \sigma^2 = 0.44543$ (bubbles). In the left column of figure 9 the corresponding snapshots for the *confined* system at similar fluid densities are presented. From a simple visual inspection one can already infer that our particular type of confinement tends to favor the formation of droplets over the percolating structures; only for higher fluid densities signatures for stripe formation within

the pores are observed. Our qualitative observations are also reflected in the corresponding pair distribution functions and the structure factors, collected in the second and third columns of figures 7 and 9. These graphs show the distinct signatures of clustering [10, 11, 31, 32], namely the presence of a huge prepeak in $S(q)$ and a wide maximum in $g(r)$ at intermediate distances corresponding to the inter-cluster separation. Furthermore, in the pair distribution function we can observe two different modulations: a short-ranged one that reflects the local structure of the fluid with a periodicity of approximately σ and a long-ranged modulation due to the pattern structure. This mesophase structure is more pronounced in droplets, whose $g(r)$ exhibit a small minimum around $r \simeq 6\sigma$ corresponding to the average diameter of the clusters. The maximum around $r \simeq 11\sigma$ indicates, as mentioned, the average distance between neighboring clusters. At very low densities and temperatures, the size of the clusters is essentially determined by the position of the maxima in $\Phi(r)$, (i.e. where $d\Phi(r)/dr = 0$); in our case this distance is $\approx 4.16\sigma$. This quantity defines approximately the average size of a cluster for low densities, which in turn conditions the inter-cluster separation in combination with the range of

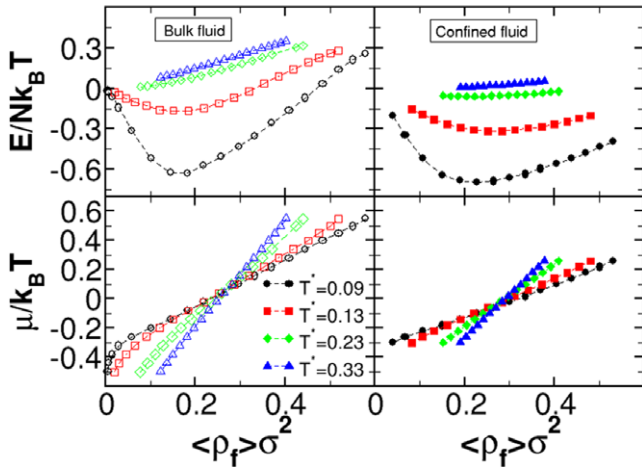


Figure 8. Adsorption isotherms $\mu/k_B T$ (lower graphs) and reduced, dimensionless internal energy, $E/Nk_B T$, (upper graphs) versus the fluid density $\langle \rho_f \rangle \sigma^2$ for the SALR fluid in the bulk (left panel) and under confinement (right panel); temperatures are labeled. Fluid densities for the confined case are calculated taking into account the area accessible to the fluid particles in the porous matrix. Error estimates of the densities are the same size as the symbols. Lines are drawn as a guide to the eye.

the repulsive tail. In our case, modifying R_c from 7.5σ to 30σ changes the average interparticle separation from 9.3σ to 11.6σ . Larger densities increase the average cluster size but hardly influence the inter-cluster separation.

In the stripe phase the maximum in $g(r)$ is still clearly visible, reflecting the average distance between stripes. In the presence of the matrix, the essential features can be observed but now the stripe phase no longer occurs as a percolating mesophase. In figure 9 one can identify the emergence of a stripe phase in the largest portion of the pore. Its growth is limited by confinement and the upper part of the pore is filled with a bubble-like phase. As a consequence of the presence of stripes, the long range maximum in $g(r)$ is found again, similar to the stripe phase of the unconfined system at $\langle \rho_f \rangle \sigma^2 = 0.296$, shown in the central panel of figure 7.

The structure factor $S(q)$ is shown for the bulk SALR fluid in the last column of figure 7 and for the confined fluid in the last column of figure 9. This function provides via a prepeak at low q -values evidence for the occurrence of a mesophase at an intermediate range. In the confined case we observe a marked growth in $S(q)$ as $q \rightarrow 0$, i.e. a characteristic feature of the presence of a porous structure with long-ranged correlations induced by the matrix. By construction these correlations have in our case the same range as the spatial extent of the simulation box, since they result from the proximity of the spinodal decomposition of the non-additive hard disk mixture, i.e. the precursor of our matrix. Furthermore, we observe both in the bulk and in the confined case a prepeak in $S(q)$ at $q \simeq 0.5\sigma^{-1}$, i.e. the signature of intermediate range order. The position of this prepeak corresponds in real space to correlations at distances $r \simeq 11\sigma$ which are in agreement with the distance at which a maximum in $g(r)$ is observed. It is worth mentioning that in the bulk bubble phase $S(q)$ also shows a prepeak, reflecting correlations between bubbles. However, the corresponding intermediate range maximum of $g(r)$ is

missing, a feature which can be considered as a signature of the bubble phase.

3.3. Structural phase diagram

We have simulated a large number of states at different temperatures and chemical potential; by identifying the different types of mesophase structures we could construct a structural phase diagram. These investigations are based on GCMC simulations extending over 5×10^5 equilibration steps followed by a run over 6×10^6 steps (2×10^6 for the confined fluid) of which 5×10^3 independent configurations were used in the cluster analysis.

We have performed a geometric cluster analysis of our configurations [33], using as link distance $r_{cl} = 2.78\sigma$, i.e. an r -value which corresponds to the point where $\Phi(r_{cl}) = 0$ (see equations (1) and (2) and figure 6). For smaller distances the potential of two interacting particles is negative and particles are thus considered to belong to the same cluster. We have calculated the cluster size distribution, $n(s)$ and its normalized counterpart, $N(s)$, as proposed by Stauffer [34]; this quantity is defined as the fraction of particles contained in clusters of size s , normalized by the cluster size, s and by the number of particles of the system, N . This normalized function has been used in a large number of publications on percolation (see, for instance, [33, 35, 36]).

In figure 10 we have plotted $N(s)$; this distribution allows us to distinguish the different types of possible mesophase structures for the bulk SALR fluid. For each type of mesophase a characteristic snapshot is shown on the lower part of this figure. Analysis of $N(s)$ leads to the definition of four distinctively different morphologies: (i) the dispersed fluid (mainly consisting of monomers), for which the cluster size distribution has a maximum at $s = 1$ and then decreases monotonically (red line in figure 10); (ii) the clustered fluid, consisting of finite size clusters where the cluster size distribution has a maximum for $s > 1$ and then decreases monotonically (blue line in figure 10); (iii) and (iv) two different percolating states, where $N(s)$ exhibits maxima at cluster sizes close to the system size: in the case of random percolated states (bubbles) all the particles belong to the same cluster (pink line in figure 10) and $N(s)$ has a single maximum; finally, in the case of cluster percolated states (stripes, green line in figure 10) secondary maxima at given large s -values resulting from the presence of disconnected stripes in the sample.

Based on this analysis, we have mapped out the different regions in the phase diagram where different mesophase structures can be identified. In figure 11 the emerging structural phase diagram for the bulk fluid (upper graph) and the confined system (lower graph) are displayed. Comparing both graphs, we observe that the cluster percolated states dominate the structural phase diagram of the confined fluid. These states correspond essentially to stripe phases in which the stripes are prevented from organizing themselves in a lamellar phase due to the effect of the matrix disorder, despite the relatively large size of the pores of our particular matrix. In a lamellar phase such as the one depicted in the lower panel of figure 10 one

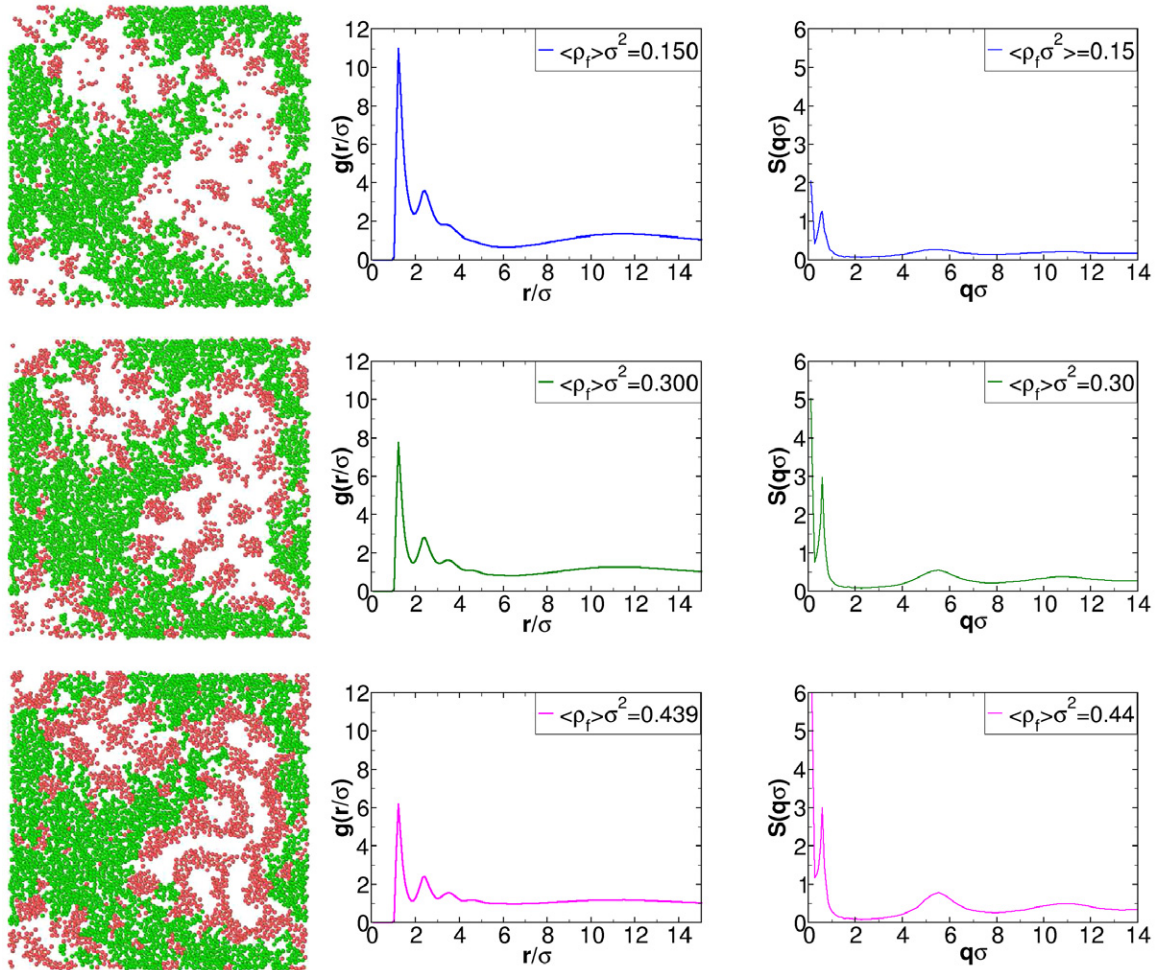


Figure 9. The same as figure 7 for the fluid confined in the porous matrix. Average fluid densities, $\langle \rho_f \rangle \sigma^2$, are indicated in the graph legends.

can see that the stripes percolate, which is not the situation in a prototype stripe phase such as the one illustrated in the lower left panel of figure 9. In the case of the confined fluid, the cluster percolated phases are mostly composed of finite size stripes.

Interestingly, the cluster fluid phase is nonetheless supported by the presence of the matrix, a fact that already became apparent when comparing the internal energies of both systems in figure 8. On the other hand, we note that when the density increases, from a visual inspection the distinction between a confined stripe phase (a cluster percolated state) and the bubble phase (random percolated state) becomes somewhat blurred due to confinement. Some structures could be thought of either as bubbles or short stripes. The presence of a maximum in the cluster size distribution for finite s however tells us that these cluster percolated phases are more properly interpreted as short stripe phases. This is the reason why random percolated states are missing from the structural phase diagram of the confined fluid of figure 11. For fluid densities higher than those depicted in figure 11, one will certainly find random percolated states, even in the confined case for matrices with sufficiently high porosities.

A quantitative comparison of our phase diagram with the one presented in figure 1 of [32] is difficult and even

problematic since the two approaches used in the respective contributions (classical density functional theory [DFT] in [32] and simulations in the present contribution) are forced to treat the different issues of the underlying model and the ensuing problems with different strategies; this applies, for instance, to the fact (i) that the tail of the potential beyond the hard core is treated in DFT in a perturbative fashion, (ii) that we consider a harshly repulsive, but soft core for the interaction or (iii) that DFT investigations are based on well-defined regular mesophases, while we have to extract the type of the mesophases from the simulation data via suitable algorithms. On a *qualitative* level we can confirm the characteristic sequence of emerging mesophases with increasing density.

3.4. Two-dimensional density distribution

In figure 12 we show the two-dimensional fluid density distribution, $\rho_f(x, y)$, at a sufficiently low temperature ($T^* = 0.12$), illustrating the effects of clustering at a rather low ($\langle \rho_f \rangle \sigma^2 = 0.067$) and a relatively high density ($\langle \rho_f \rangle \sigma^2 = 0.29$); the density of the porous matrix is $\rho_m \sigma^2 = 0.324$. In these figures the black area represents those regions from which the centers of the fluid particles are excluded, i.e. where $\rho_f(x, y) = 0$.

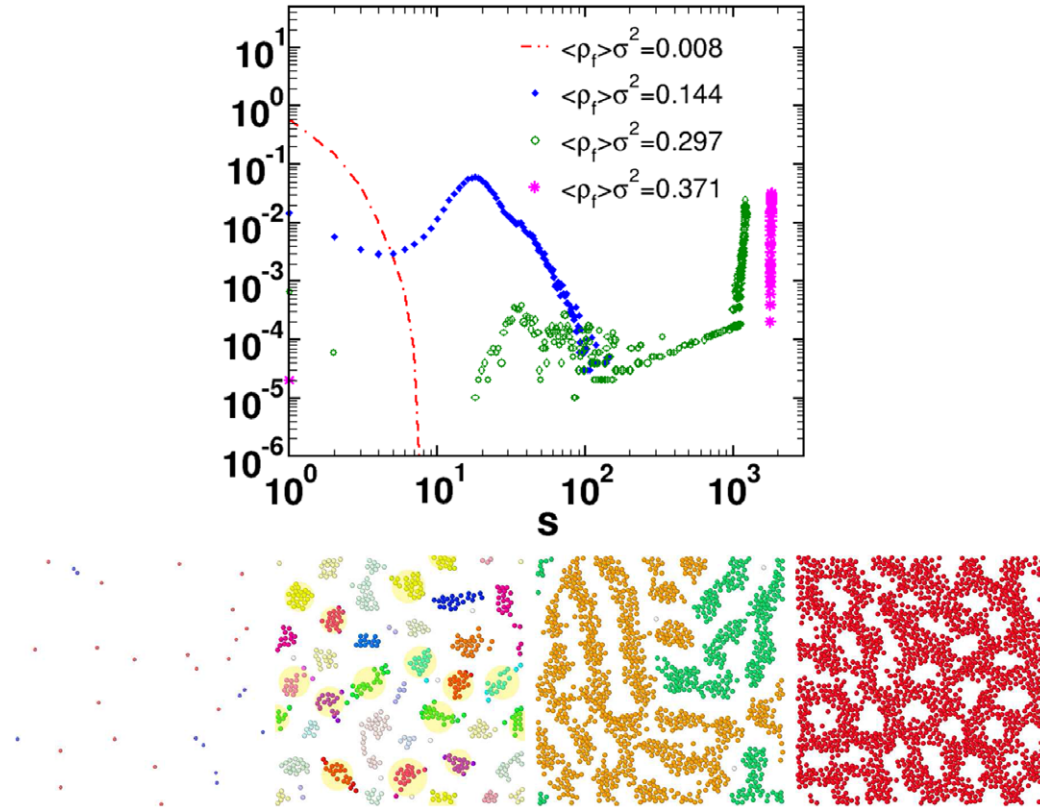


Figure 10. The upper panel shows the normalized cluster distribution $N(s)$ (see text) for various fluid densities $\langle \rho_f \rangle \sigma^2$ of the SALR fluid as labeled. Representative snapshots of the corresponding mesophases are illustrated in the bottom panels (from left to right with increasing $\langle \rho_f \rangle$). Different colors of the particles provide an approximate measure of how many particles are involved in separated regions of the respective mesophases.

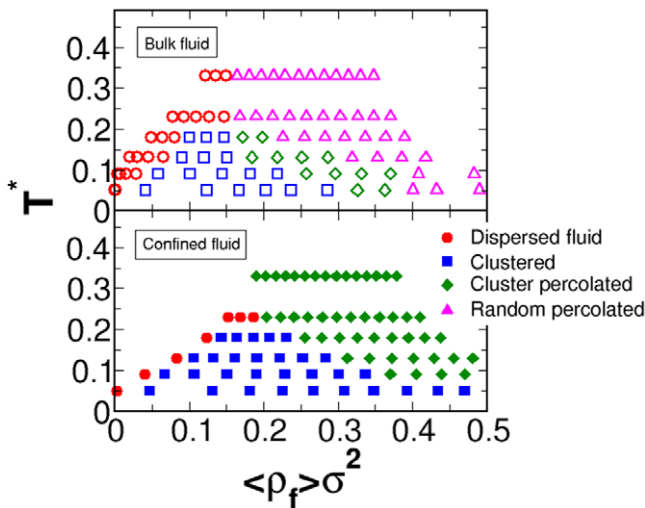


Figure 11. Structural phase diagram of the bulk SALR fluid (upper graph) in the $(T^*, \langle \rho_f \rangle)$ -plane. The lower graph corresponds to the phase diagram for the confined fluid. Different mesophases are indicated on the figure by different symbols and colors as labeled (open symbols—bulk fluid, full symbols—confined fluid).

The formation and the evolution of the clusters in these systems are relatively slow processes, in particular when the clusters are trapped in narrow regions which hinder their moves. Therefore, we require rather long GCMC simulations to obtain an exhaustive sampling of the configurational space

that allows us to draw a sufficiently smooth density distribution. With this requirement in mind, we have performed 5×10^5 steps for equilibration and 4×10^6 steps to accumulate and to analyze the configurations after every 200 steps.

The right panel of figure 12 corresponds to the higher fluid density: here the pores are almost filled and we can observe that the arrangement of the minima and of the maxima in the density distribution approaches the typical pattern of a triangular lattice. Density maxima (marked in yellow) correspond essentially to individual particles. From this panel one can see that the highest values for the fluid density are observed close to the pore walls. This might seem astonishing at first sight since the matrix-fluid interaction is entirely repulsive. However, this alleged contradiction can easily be explained: since the fluid particles attempt to minimize their mutual long-range repulsion, they move as far apart as possible from each other enhancing thereby the fluid density close to the walls; this feature, in turn, lowers the internal energy since typical interparticle separations are then below r_{cl} . This explains why for low temperatures we have seen that in contrast with the bulk, now the internal energy remains negative for all fluid densities under consideration. Our observation that the particles tend to assemble close to the matrix, is similar to results reported some time ago in [12]: an enhanced fluid density was also observed for a SALR fluid confined between two walls when their separation was incommensurate with the periodicity of the mesophase of the bulk system.

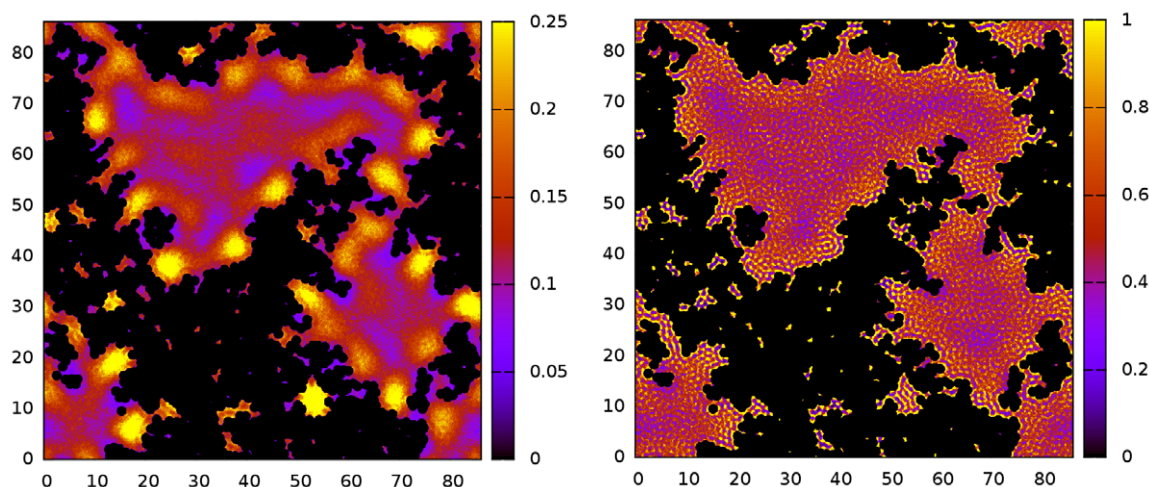


Figure 12. Two-dimensional contour plot of the density distribution $\rho_f(x, y)$ of the SALR fluid adsorbed in a disordered, porous matrix for $\langle \rho_f \rangle \sigma^2 = 0.067$ (left panel) and $\langle \rho_f \rangle \sigma^2 = 0.29$ (right panel); the height of $\rho_f(x, y)$ is color-coded via the bars on the right hand sides of the panels. The left panel corresponds to a cluster phase, while the right panel is a typical stripe (cluster percolated) state point. In both cases the matrix density is $\rho_m \sigma^2 = 0.324$ and the temperature was set to $T^* = 0.12$. The black area represents those regions from which the centers of the fluid particles are excluded, i.e. where $\rho_f(x, y) = 0$.

The left panel of figure 12 corresponds to the lower fluid density case. Here we observe that the density distribution provides evidence of regions of high fluid density that are spatially well-separated, corresponding to well-defined particle clusters. These aggregates tend to populate certain ‘pockets’ of the porous matrix: while the short-range attractive part of the potential $\Phi(r)$ is responsible for the cluster formation, the long-range part of the interaction induces the repulsion between clusters; thus the ‘preferred’ positions of the clusters within the porous structure are those where the matrix is able to screen the long-ranged repulsive interaction between the clusters.

The distance between neighboring clusters—defined as the average separation between the density maxima in figure 12—agrees well with the values obtained from the position of the prepeak in $S(q)$ and location of the wide maxima in $g(r)$, i.e. at distances $r \sim 10\sigma - 11\sigma$ of the confined system. This inter-cluster distance is also in accordance with the typical inter-cluster distances observed in the bulk fluid. This average separation is exclusively determined by the balance of range and intensity of the repulsive and attractive components of the SALR interaction: it is hence unaffected by the presence of the otherwise inert matrix.

4. Conclusions

In summary, we have observed that the adsorption process of the SALR fluid in our porous matrix strengthens the formation of droplets, i.e. it stabilizes the cluster phase and impedes the formation of percolating structures. Emerging stripe phases can still be found in large pores, whereas in small pores the cluster phase transforms into a bubble phase upon increasing fluid density. For the type of matrix we constructed, we find that the pores are wide enough to preserve the average inter-cluster separation in the confined fluid with values quite close to those obtained for the infinite fluid.

Future work will concentrate on the effects of confinement on the fluid dynamics and the modulation of the fluid mesophases by tuning of the matrix-fluid interactions, possibly including the presence of heterogeneities in the matrix composition.

In addition to the ‘terrestrial’ applications of fluids adsorbed and included in disordered porous matrices one might speculate that similar mechanisms might be observed at atmospheric density variations close to planetary objects, leading eventually to condensation.

Acknowledgments

CB, NGA and EL acknowledge financial support from the Dirección General de Investigación Científica y Técnica under Grants No. FIS2010-15502 and FIS2013-47350-C5-4-R and from the CSIC in the form of the project PIE 201080E120. GK acknowledges financial support from the Austrian Science Fund (FWF) under Project Nos. P23910-N16 and F41 (SFB ViCoM). We are grateful to Claudio Martín (Madrid) and to D F Schwanzer and J Kurzidim (both Wien) for helpful scientific discussions.

References

- [1] Haller W 1965 *Nature* **206** 693
- [2] Corma A 1997 *Chem. Rev.* **97** 2373–420
- [3] Haller W 1965 *J. Chem. Phys.* **42** 686
- [4] Levitz P, Ehret G, Sinha S K and Drake J M 1991 *J. Chem. Phys.* **95** 6151
- [5] Delaunay B 1934 *Bull. Acad. Sci. URSS* **6** 793–800
- [6] Torquato S 2001 *Random Heterogeneous Materials* (New York: Springer)
- [7] Almarza N G, Gallardo A, Martín C, Guil J M and Lomba E 2009 *J. Chem. Phys.* **131** 244701
- [8] Kurzidim J and Kahl G 2011 *Mol. Phys.* **109** 1331–42
- [9] Sear R P, Chung S W, Markovich G, Gelbart W M and Heath J R 1999 *Phys. Rev. E* **56** R6255

- [10] Imperio A and Reatto L 2004 *J. Phys.: Condens. Matter* **16** S3769
- [11] Imperio A and Reatto L 2006 *J. Chem. Phys.* **124** 164712
- [12] Imperio A and Reatto L 2007 *Phys. Rev. E* **76** 040402
- [13] Mulheran P, Pellenc D, Bennett R, Green R and Sperrin M 2008 *Phys. Rev. Lett.* **100** 068102
- [14] Stradner A, Sedgwick H, Cardinaux F, Poon W C K, Egelhaaf S U and Schurtenberger P 2004 *Nature* **432** 492
- [15] Porcar L, Falus P, Chen W R, Faraone A, Fratini E, Hong K, Baglioni P and Liu Y 2010 *J. Phys. Chem. Lett.* **1** 126
- [16] Cardinaux F, Zaccarelli E, Stradner A, Bucciarelli S, Farago B, Egelhaaf S U, Sciortino F and Schurtenberger P 2011 *J. Phys. Chem. B* **115** 7227
- [17] Yadav S, Laue T M, Kalonia D S, Singh S N and Shire S J 2012 *Mol. Pharmacol.* **9** 791
- [18] Meyra A G, Zarragoicochea G J and Kuz V A 2012 *Mol. Phys.* **110** 173–8
- [19] Gelb L and Gubbins K 1998 *Langmuir* **14** 2097–111
- [20] Siggia E 1979 *Phys. Rev. A* **20** 595
- [21] Jung J, Jhon M and Ree F 1989 *Chem. Eng. Sci.* **44** 1829–35
- [22] Kofke D and Glandt E 1988 *Mol. Phys.* **64** 1105
- [23] Frenkel D 1993 *Computer Simulation in Chemical Physics* ed M P Allen and D J Tildesley (Dordrecht: Kluwer)
- [24] Lomba E, Alvarez M, Lee L and Almarza N 1995 *J. Chem. Phys.* **104** 4180–8
- [25] Ferreira A and Prodanescu E 2005 *Int. J. Mod. Phys. C* **16** 45–61
- [26] Sink'o K, Torma V and Kov'acs A 2008 *J. Non Cryst. Solids* **354** 5466
- [27] Lomba E, Bores C and Kahl G 2014 *J. Chem. Phys.* **141** 164704
- [28] Tanemura M, Ogawa T and Ogita N 1983 *J. Comput. Phys.* **51** 191–207
- [29] Imperio A, Pini D and Reatto L 2006 *Int. Workshop on Collective Phenomena in Macroscopic System (Villa Olmo, Como, Italy, 4–6 December 2006)*
- [30] Schwanzer D and Kahl G 2011 *Condens. Matter Phys.* **14** 33801
- [31] Schwanzer D F and Kahl G 2010 *J. Phys.: Condens. Matter* **22** 415103
- [32] Archer A 2008 *Phys. Rev. E* **78** 031402
- [33] Godfrin P, Castañeda-Priego R, Liu Y and Wagner N 2013 *J. Chem. Phys.* **139** 154904
- [34] Stauffer D 1979 *Phys. Rep.* **1** 1–74
- [35] Wang J 1989 *Phys. A: Stat. Mech. Appl.* **161** 249–68
- [36] Chen S, Rouch J, Sciortino F and Tartaglia P 1994 *J. Phys.: Condens. Matter* **6** 10855–83